CrossMark

TRANSACTIONAL PROCESSING SYSTEMS

Mass Detection in Mammographic Images Using Wavelet Processing and Adaptive Threshold Technique

P. S. Vikhe[1] · V. R. Thool[1]

Abstract Detection of mass in mammogram for early diagnosis of breast cancer is a significant assignment in the reduction of the mortality rate. However, in some cases, screening of mass is difficult task for radiologist, due to variation in contrast, fuzzy edges and noisy mammograms. Masses and micro-calcifications are the distinctive signs for diagnosis of breast cancer. This paper presents, a method for mass enhancement using piecewise linear operator in combination with wavelet processing from mammographic images. The method includes, artifact suppression and pectoral muscle removal based on morphological operations. Finally, mass segmentation for detection using adaptive threshold technique is carried out to separate the mass from background. The proposed method has been tested on 130 (45+85) images with 90.9 and 91 % True Positive Fraction (TPF) at 2.35 and 2.1 average False Positive Per Image(FP/I) from two different databases, namely Mammographic Image Analysis Society (MIAS) and Digital Database for Screening Mammography (DDSM). The obtained results show that, the proposed technique gives improved diagnosis in the early breast cancer detection.

This article is part of the Topical Collection on *Transactional Processing Systems*

✉ P. S. Vikhe
pratap_vikhe@yahoo.co.in

V. R. Thool
vrthool@yahoo.com

1 Shri Guru Gobind Singhji Institute of Engineering and Technology, Nanded, India

Introduction

The cancer is uncontrolled growth of cells in a particular location of the body. Most frequent cancer diagnosed in women is the breast cancer, leading cause of death among women [11]. One out of eight womens in the United States (US) will develop breast cancer at some stage during her life time according to *National Cancer Institute* [25, 34]. According to World Health Organization (WHO), cancer accounted 13 % of all deaths in the world in 2004 [34]. Breast cancer cases and deaths estimated by *American Cancer Society* (ACS), yearwise of US are mentioned in Table 1 [3]. At present, there are no effectual methods to avert breast cancer, as its cause remains unknown. Detection of breast cancer at early stages is the only solution to reduce the mortality rate and give chance to recover from the cancer [34]. To detect breast cancer at early stage, X-ray mammography is used as a diagnostic and screening tool by radiologist. This is the most reliable technique for early detection of breast cancer, reducing the mortality rates up to 25 %. Screening mammography is not easy task for radiologists, 10–30 % of lesions are missed during routine screening [11, 17, 25].

The signs of breast cancer are masses and micro-calcifications. A small abnormal deposit of calcium in the breast appears as a small bright spot, is often a sign of a micro-calcification, and the average size is about 0.3 mm. The potential abnormality on a mammogram is the sign of mass. The masses are of two different types, one is malignant, which has an irregular edges or a star-burst appearance and another is benign, which have a smooth, well-defined

Table 1 Estimated cases and deaths of breast cancer yearwise

Year	Estimated new cases			Estimated deaths		
	Both sex	Male	Female	Both sex	Male	Female
2005	2,12,930	1,690	2,11,240	40,870	460	40,410
2006	2,14,640	1,720	2,12,920	41,430	460	40,970
2007	1,80,510	2,030	1,78480	40,910	450	40,460
2008	1,84,450	1,990	1,82,460	40,930	450	40,480
2009	1,94,280	1,910	1,92,370	40,610	440	40,170
2010	2,09,060	1,970	2,07,090	40,230	390	39,840
2011	2,32,620	2,140	2,30,480	39,970	450	39,840
2012	2,29,060	2,190	2,26,870	39,920	410	39,510
2013	2,34,580	2,240	2,32,340	40,030	410	39,620
2014	2,35,030	2,360	2,32,670	40,430	430	40,000

edges. They are of three different sizes, small (3 to 15 mm), medium (15 to 30 mm), and large (30 to 50 mm). They are also of varying shape, and density with low contrast bounded by non-uniform tissue background with same characteristics that of supporting tissues [17, 19, 21, 25, 33, 34]. Hence mass enhancement and detection are the challenging task compared to micro-calcification enhancement and detection.

To improve the diagnostic performance of radiologists, various Computer-Aided Diagnosis (CAD) methods are proposed and can be found in the literature [12, 13, 16, 17, 24, 25, 35]. Pelin Gorgel et al. [13] proposed a method using wavelet transform and Homomorphic filtering for enhancement and denoising of mammograms.This method has limited effect on highly dense breast, as dense tissue and mass having almost same contrast. A. Mencattini et al. [25] proposed an algorithm for denoising of mammograms using local iterative noise variance estimation, and micro-calcification enhancement based on adaptive gain setting for mammographic image. Also a novel segmentation method was proposed in combination with dyadic wavelet and morphological operations for mass detection. The over segmentation of mass may be possible in case of dense-glandular mammograms with this approach. A new method based on morphological component analysis proposed by Xinbo Gao et al. [12], which uses decomposition of the mammographic images into piecewise-smooth and texture component. In this concentric layer criteria is used to detect different types of doubtful area in mammograms. This approach may have limited effect, when the mass is hidden in the surrounding breast tissue, due to low contrast. Maciej A. Mazurowski et al. [24] presented a CAD system using template matching scheme for mammographic mass detection based on intelligently selected templates. This technique have less effect on benign masses as compare to malignant masses. A non-linear enhancement in homomorphic filtering and denoising of mammographic images based on wavelet processing was proposed by Jeong Hyun YOON et al. [35]. The results with this technique is unsatisfactory in case of fatty-glandular and dense-glandular mammograms, as it emphasize entire high contrast region from image. Yoshitaka Kimori [16] suggested a new method, Rotational Morphological Processing (RPM) for enhancing features of masses and abnormalities in medical images, including extraction of desired features by mathematical morphology. However, with this approach boundaries may not be correctly identified when suspicious region are invisible and embedded in surrounding breast tissue due to poor contrast. An algorithm based on linear transformation enhancement filter and adaptive threshold technique was developed by Guillaume Kom et al. [17] for automatic detection of mass in mammographic image. However, linear filter enhancement technique has a partial effect on extremely dense mammograms, as suspicious mass and high density tissue has similar characteristics.

Considering above facts, in this paper, we have proposed a simple algorithm for mass enhancement and detection for mammographic images using wavelet processing and adaptive threshold technique. The algorithm includes pre-processing, wavelet based denoising, enhancement, and finally mass segmentation using adaptive thresholding.

The paper is organized as follow. Section "Introduction", presents introduction with current literature studies. Section "Methodology" describes the concept of wavelet based denoising and enhancement for mammographic images and segmentation. Experimental results and discussion based on the proposed method are demonstrated in section "Experimental Results" and "Discussion". Conclusion drawn based on the above experimentation is given in section "Conclusion".

Methodology

Pre-Processing

The pre-processing is followed by artifact suppression and pectoral muscle segmentation. The region emerges triangular area across the upper posterior periphery of the image on a proper Medio-Lateral Oblique (MLO) as a high intensity connecting to the chest is called pectoral. Pectoral muscle is captured, while acquiring the mammogram, affects the detection of suspicious mass during processing of mammograms. Hence, pectoral muscle including radiopaque artifacts i.e. (labels, wedges, etc.) shown in Fig. 1a should be removed for better detection of lesions from mammographic images [10, 20, 26]. In this work, all the mammographic images are made right oriented, so that pectoral muscle appears at the left corner of the mammograms and segmentation becomes easier. To achieve this task vertical centroid and mean of the images are computed of the left and right half. If the left half mean is greater than right half mean, flip the image I else retain the image I.

Artifact Removal

The following steps are applied for the removal of artifacts in the mammographic images:

Step 1: Convert mammographic image I to binary image I_{bi} using threshold technique, providing number of objects (artifacts and breast region) as an output.

Step 2: The morphological erosion [28, 30] is applied on I_{bi} to disconnects the objects obtained in step 1 from each other providing I_{er}.

$$I_{er} = I_{bi} \oplus B = \left\{ p \in Z^2|_{p=i+b,} \atop i \in I, b \in B \right\} \quad (1)$$

Where, I_{bi} is binary image, I_{er} is morphological eroded image, B is structuring element, p is set of points, b is element in B, and Z^2 is two dimensional space.

Step 3: Computing the size of each object obtain in step 2 for I_{er}, removing all small objects and considering only the large object inside the image I_{er}, which is the breast region with sharp boundaries I_{sb}.

Step 4: The sharp boundary is the output of step 3 denoted as I_{sb} (sharp boundary image). To smooth this breast boundaries, morphological dilation [28, 30] is applied on the I_{sb} image, which provides breast region white and background region black as an output.

$$I_{di} = I_{sb} \ominus B = \left\{ p \in Z^2|_{p=i+b \in I}, \text{ for every } b \in B \right\}$$

Where, I_{di} is morphological diluted image i.e. (breast region image), B is structuring element, p is set of points, b is element in B, and Z^2 is two dimensional space.

Step 5: The pixel value 1 (white) is replaced by corresponding pixel value of original image I in binary mask generated I_{di} in step 4, to extract the original pixel value of the image I_a, where, I_a is artifact remove image.

Figure 1b shows an example for artifact removal from mammographic images.

Pectoral Muscle Segmentation

In mammogram, pectoral muscle appears approximately with the same density as a dense tissue of the breast. This, affects the detection process of breast cancer. Therefore, pectoral muscle segmentation is important, to find the breast abnormalities only in the breast region. The process of removing pectoral muscle is given below:

Step 1: Using morphological reconstruction by dilation of a structuring element, B form the artifact removed image, I_a consists in iterative sequences of elementary dilation's and point-wise image transformations [30]. In this, backward ($K_8^{\leftarrow}$) and forward ($K_8^{\rightarrow}$) neighbors are used for forward and backward scans respectively. Thus desired

Fig. 1 **a** Original image **b** artifact suppressed image and **c** pectoral muscle removed image

Original Image   Artifcat Supressed Image   Pectoral Muscle Removed

Artifact

Pectoral Muscle

a   **b**   **c**
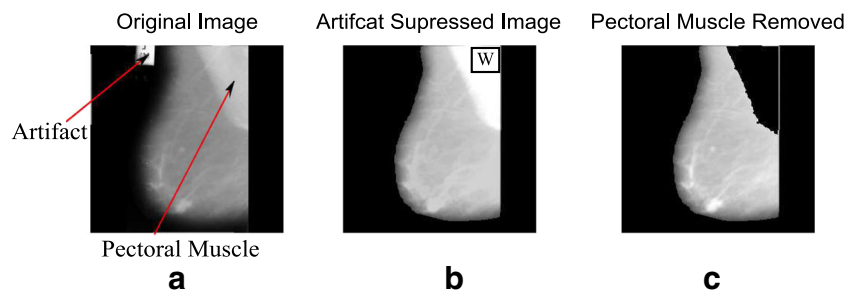
reconstruction of the artifact removed image I'_a is obtained as [30].

– Forward scan of all pixels p

$$I'_a(p) \leftarrow min\left[B(p), max\left\{I_a(b) \mid b \in K_8^{\leftarrow}(p) \cup p\right\}\right]; \tag{2}$$

– Backward scan of all pixels p

$$I'_a(p) \leftarrow min\left[B(p), max\left\{I_a(b) \mid b \in K_8^{\rightarrow}(p) \cup p\right\}\right]; \tag{3}$$

Step 2: Then subtract artifact removed image, I_a from morphological reconstructed image, I'_a to have reduced contract of region of interest and retain the intensity of pectoral region, I_b.

Step 3: Select the area of 61×61 in the region of pectoral muscle as a window, W. Apply this window from the first row of the image I_a obtained in step 2 and this can be seen in Fig. 1b.

Step 4: Finding the maximum intensity of the I_a image area of 61×61 in the region of pectoral muscle obtained in step 3. Hence, computed threshold, is $T_p = max(W)$.

Step 5: Applying this value of threshold, T_p to I_b obtained in step 2 for removal of pectoral muscle, by the following operation,

$$I_{pm}(x, y) = \begin{cases} 0, & I_b(i, j) \leq T_p \\ 255, & \text{otherwise.} \end{cases} \tag{4}$$

where $I_{pm}(i, j)$ is an image with pectoral region only.

Step 6: Finally, the pectoral muscle segmented image I_P can be obtained as;

$$I_P(i, j) = \begin{cases} I_{pm}(i, j) = 0, & I_{pm}(i, j) > 1 \\ I_{pm}(i, j) = I_a(i, j), & \text{otherwise.} \end{cases} \tag{5}$$

Figure 1c shows an example for the pectoral muscle segmentation which is further used for mass enhancement using wavelet processing.

Quantitative Analysis of Pectoral Segmentation

In this work, the author has manually drawn the pectoral boundary and check by radiologist to have standard pectoral muscle or ground truth for the MLO view of each mammogram. The two parameters False positive (FP) rate and False Negative (FN) rate are used for quantitatively evaluate the accuracy of pectoral muscle segmentation [5]. The FP and FN rate are defined as below:

▷ False positive (FP) pixels: The pixels detected in pectoral muscle other than or outside ground-truth or reference region, computed in percentage using Eq. 6.

$$\text{Percentage FP pixel} = \frac{|A_1 \cup A_2| - |A_2|}{|A_2|} \times 100\% \tag{6}$$

▷ False negative (FN) pixels: The pixels outside the detected pectoral region but inside the ground truth region, computed in percentage using Eq. 7.

$$\text{Percentage FN pixel} = \frac{|A_1 \cup A_2| - |A_1|}{|A_2|} \times 100\% \tag{7}$$

where, $A_1 \in$ detected pectoral region pixels set and $A_2 \in$ reference or ground-truth pectoral region pixels set.

The pectoral muscle segmentation approach were tested for 75 images form MIAS (45) and DDSM (35) database respectively from entire data-set that is used for mass detection. The 93.4 % results were acceptable (i.e. 70 images pectoral were detected from 75 images) and 6.6 % results were unacceptable (i.e. 5 images pectoral were not detected from 75 images). The mean FP rate were 1.87 and mean FN rate were 7.58 for pectoral muscle segmentation approach.

Wavelet Based Denoising and Enhancement

The wavelet transform is the best tool for the analysis as it represents the significant information at different resolutions and levels, having orthogonal and bi-orthogonal bases used in various applications [21, 23, 29]. Decimated wavelet transform has the limitation that, it produces a large number of artifacts, while reconstruction of the wavelet coefficients after processing. For example, Gibbs phenomena in the neighborhood of discontinuities to the lack of translation invariance of the wavelet basis [6]. As per Jean-Luc Starck et al. [31] Haar filters are very useful for denoising; whereas the results of denoising can be improved more than 2.5 dB using undecimated wavelet transform [25]. In undecimated analysis, each band has the same size as the original image, which is implemented using Haar filter. The schematic representation of wavelet based denoising and enhancement is shown in Fig. 2, where $\tilde{g}(\omega)$ and $\tilde{h}(\omega)$ are forward filters and $\tilde{k}(\omega)$ and $\tilde{l}(\omega)$ are inverse filters. Figure 2 consist of three parts decomposition, enhancement followed by reconstruction and explained as follow.

Wavelet Based Denoising

In X-ray images denoising is complicated task due to following reasons:

1. No absolute boundary to distinguish an information from noise.
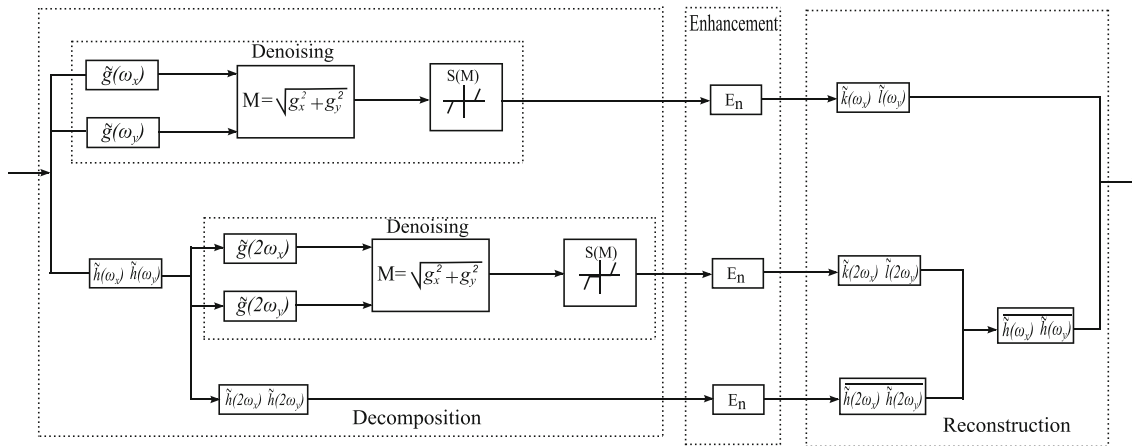2. It is impractical to completely remove the noise from features of interest.

Fig. 2 Schematic representation of wavelet based denoising and enhancement (two levels decomposition and reconstruction)

Hence, enhancement process is dominated due to the presence of noise. However, denoising technique based on the amendment of the wavelet coefficients is used. The gradient operator is applied on the detail coefficients of wavelet transform, as it exhibits higher signal to noise ratio (SNR) [25]. Then the shrinkage operator [8] is applied on the magnitude of the gradient coefficients M. To avoid the artifact introduction, shrinkage operator used is monotonically non-decreasing and piecewise linear function [9]. This is represented in the decomposition block of Fig. 2.

The shrinkage function used for denoising is given by Eq. 8,

$$S(M) = sign(M) \begin{cases} \mid M \mid -T_n , & \mid M \mid \geq T_n \\ 0, & \text{elsewhere.} \end{cases} \quad (8)$$

where $S(M)$ is the shrinkage operator, M is the magnitude of the gradient coefficient, and T_n is the threshold. Threshold T_n, play a vital role, in the depiction of edges. Large value produces blurring of small edges, while a small value does not remove sufficient noise [25]. Hence, selection of T_n is an important parameter in shrinkage operator. As per [7] T_n is selected as Eq. 9,

$$T_n = \sigma \sqrt{2log(N)}/\sqrt{N} \quad (9)$$

where N is the length of the signal and σ is the standard deviation of coefficients.

Wavelet Based Enhancement for Mass Detection

Enhancement is the process of improving the quality of the image. The mapping of wavelet coefficients can be made by using linear function $E_n = K_n x$ for linear enhancement, where K_n denote the gain and x, wavelet coefficients. The linear enhancement corresponds to an unsharp masking integrates at each level [9]. To overcome the loss of details

due to saturation of high value coefficients after reconstruction process, design of nonlinear enhancement function is essential, which should fulfill the following constraints.

1. Coefficient with small value should have high gains to enhance low contrast region than that of high contrast
2. To avoid artifacts introduced during analysis and synthesis, non-linear function $E_n(x)$ has to be continuous and monotonically increasing.
3. There should not be blurred sharp edges.

Thus, to satisfy the above requirement, we used Eq. 10, as a piecewise linear operator $E_n(x)$ for mass enhancement with constant gain [25]. As the masses are of varying size, shape, and density, low contrast, they are often overlapped with dense breast tissues. Therefore, mass detection is the challenging tasks with respect to micro-calcification. The advantage of piecewise linear operator, to reduce the low level of noise at every decomposition level. The piecewise linear enhancement operator for mass detection is given by Eq. 10,

$$E_n(x) = \begin{cases} x - (K_n - 1)(T_2 - T_1), & x < -T_2 \\ K_n x + (K_n - 1)T_1, & -T_2 \leq x \leq -T_1 \\ K_n x, & \mid x \mid < T_1 \\ K_n x - (K_n - 1)T_1, & T_1 \leq x \leq -T_2 \\ x + (K_n - 1)(T_2 - T_1), & x > T_2 \end{cases} \quad (10)$$

In this work, threshold $T_2(n)$ and K_n are the two free parameters of the enhancement operator $E_n(x)$. T_1 i.e. (T_n) and T_2 are the thresholds related to noise and saturation region respectively depends on the level n and K_n is the gain used as $K_n = K_c$ $0 \leq n \leq N - 1$, were K_c is constant and multiplied to wavelet coefficients at each level. Selection of threshold $T_1(n)$ is related to the noise computed in denoising section, and $T_2(n)$ is related to the saturation region computed using classical method as per [9], $T_2(n) = t \times max\{\mid x \mid\}$, where t is $0 < t \leq 1$ user define. The obtained enhanced image, is denoted as, I_e.

Table 2 Details of the database

Database	Mini-MIAS	DDSM
Projections	MLO	CC (50) and MLO (35)
Spatial resolution	$50\ \mu m/pixel$	$43.5,\ 50,\ 42\ \mu m/pixel$
Gray-level quantization	8 bits	12, 16 bits
Dimension	1024×1024 pixels	Variable
Digitizer	Joyce-Loebl microdensitometer	Howtek MultiRad 850, Lumisys 200
	SCANDIG-3	Laser, DBA M2100 ImageClear
Database Size	322	2620
Database Tested	45((39 with at least one lesion) + 06 Normal)	85 ((75 (47 CC+ 28 MLO) with at least one lesion)+ 10 (03 CC + 07 MLO) Normal)

Segmentation for Mass Detection

The segmentation of the mammographic image, plays a vital role in mass detection. To extract one or more region of interest (ROIs) from the background is the main aim of segmentation. This is not an easy task, due to non-uniform tissue background with similar characteristics, make it difficult to discriminate from the mammograms. Therefore, segmentation is essential for enhancement of the significant features [17, 33]. To exemplify the suspicious mass from the enhanced mammographic image, the adaptive thresholding technique is used in the present work. The selection of threshold for segmentation to separate the enhanced area from the background and surrounding tissue follows iterative procedure as below [28].

Algorithm steps:

1. Finding the minimum and maximum intensity of the enhanced image I_e.

2. Computing initial threshold T_h using Eq. 11,

$$T_h = \frac{min(I_e(i,\,j)) + max(I_e(i,\,j))}{2} \tag{11}$$

3. Compute mean of the background and object gray level μ_1 using and μ_2 respectively.

$$\mu_1 = \frac{\sum_{(i,j)\varepsilon background} I_{e_1}(i,\,j)}{\#background - pixels} \tag{12}$$

$$\mu_2 = \frac{\sum_{(i,j)\varepsilon object} I_{e_2}(i,\,j)}{\#object - pixels}, \tag{13}$$

Where I_{e_1} and I_{e_2} are background and object region of mammographic image computed using Eqs. 12 and 13, where as # background-pixels and # object-pixels are the number of background and object pixels of the image respectively.

$$I_{e_1}(i,\,j) = \begin{cases} I_e(i,\,j), & I_e(i,\,j) < T_h \\ 0, & \text{otherwise.} \end{cases} \tag{14}$$

$$I_{e_2}(i,\,j) = \begin{cases} I_e(i,\,j), & I_e(i,\,j) \geq T_h \\ 0, & \text{otherwise.} \end{cases} \tag{15}$$

4. Calculating the average of mean intensity level using Eq. 16 of the background (μ_1) and object (μ_2) to obtain new threshold T_{h_n} as,

$$T_{hn} = \frac{\mu_1 + \mu_2}{2} \tag{16}$$

5. The segmentation threshold T_h is computed as per Eq. 17, if $T_{h_n} = T_h$, stop the iteration else return to step 3. i.e.

$$T_h = \begin{cases} T_{hn}, & (T_h - T_{hn}) \geq 1 \\ T_h, & T_h - T_{hn} = 0. \end{cases} \tag{17}$$

Thus, the segmentation of enhanced mammographic image is obtained using Eq. 18,

$$I_s(i,\,j) = \begin{cases} 1, & I_e(i,\,j) \leq T_h \\ 0, & I_e(i,\,j) > T_h. \end{cases} \tag{18}$$

Where $I_s(i,\,j)$ is the segmented mass from mammographic image.

Experimental Results

The usefulness of the proposed algorithm for enhancement and detection of ROIs from mammograms is described in this section. We have tested the proposed algorithm for two

Fig. 3 Schematic representation of mass detection system
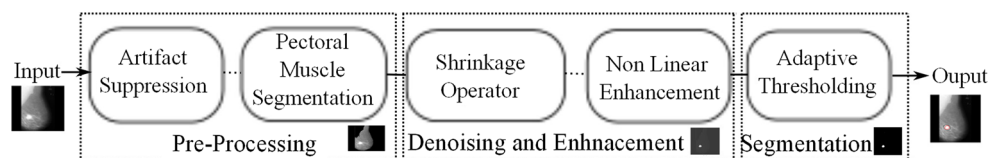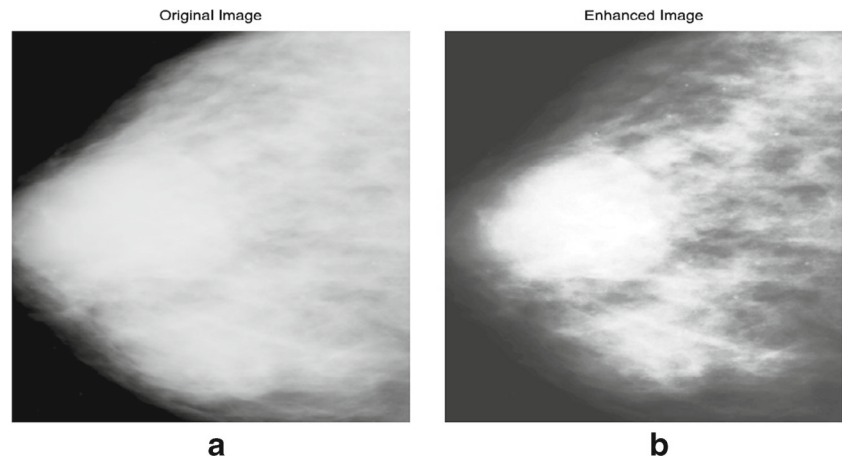
Fig. 4 **a** Original image, case B 3002(DDSM) **b** enhanced image using histogram equalization

different databases, one is MIAS and another is DDSM. The details of the database are presented in the Table 2. The MIAS and DDSM database images contain the *ground truth* information about locations of suspicious area. The DDSM database is present in two views, i.e. Cranio-Caudal (CC) and Medio-Lateral Oblique (MLO), each having two images of left and right side of the breast in Lossless Joint Photographers Expert Group (LJPEG) format along with details of the patient and abnormalities. Where as, MIAS database with only MLO view for all images with type of abnormality, and center of abnormality circle enclosing with approximate radius (in pixels) [1, 2, 32].

The key basis to authenticate or validate the results of proposed method is the information provided by radiologists and their opinions, along with the similarity measure between obtain results with ground truth. The computer aided detection system is considered as a correct if at least 50 % of region is overlapped with the true suspicious region or ground truth [15]. Thus, comparison of the obtained results for mass detection have been carried out with *ground truth* provided by MIAS and DDSM database using standard Jaccard similarity measure [14]. The Jaccard index,

$J(B_1, B_2)$ is defined as the intersection of two data sets over their union for binary variable [0, 1] computed using Eq. 19. The output Jaccard index will be 1 if the area B_1 and B_2 overlaps completely, else it will be 0 when these two areas doesn't overlaps.

$$J(B_1, B_2) = \frac{B_1 \cap B_2}{B_1 \cup B_2} \qquad (19)$$

where, $J(B_1, B_2)$ is Jaccard similarity measure, B_1 represent the ground truth, and B_2 represent the region detected by proposed method. The proposed method elaborated in Fig. 3, has correctly enhanced and detects the mass, which is greater than 50 %, with overlapping of 71 % and 76 % for MIAS and DDSM database respectively. This helps the radiologist for mass detection easily, than that of plain images. In this work to save the computation time size of mammograms have been reduced four times by taking average of 4×4 pixels and replacing it with one pixel. The proposed technique is implemented in MATLAB software R2012@a on a PC (Intel i7 3.40 GHz CPU and 8-GB RAM), with average execution time of 1.82 sec and 1.95 sec per image for MIAS and DDSM database respectively.

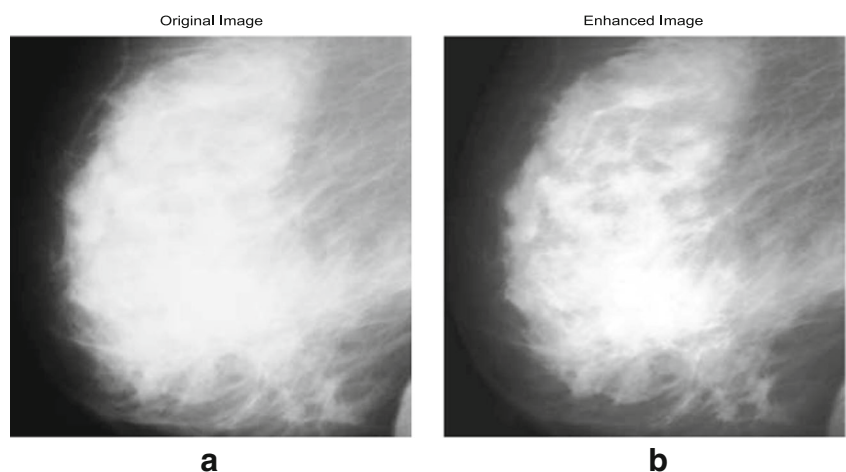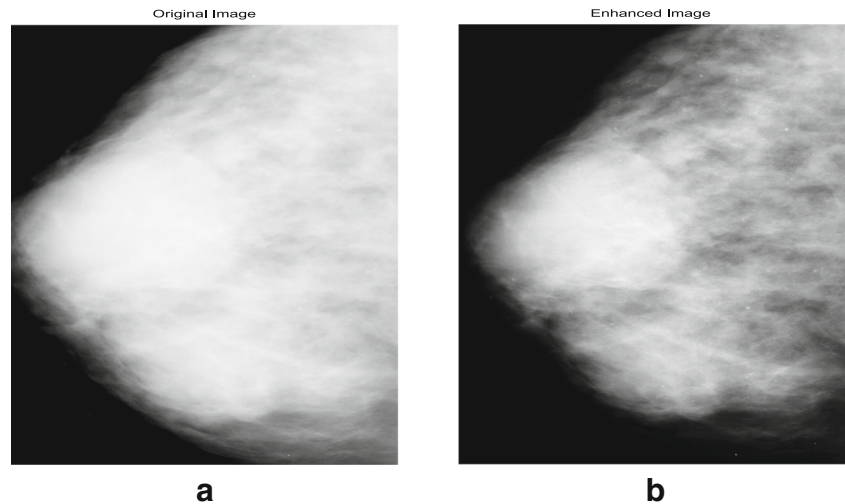**Fig. 5** **a** Original image,case mdb105(MIAS) **b** enhanced image using histogram equalization

Fig. 6 a Original image,case B 3002(DDSM) **b** results obtained using method proposed by Pelin Gorgel et al. [13]


Figures 4a and 5a shows an original dense mammograms having the ROIs hidden in dense tissue for DDSM and MIAS database, respectively. The same images have been used as a reference for the enhancement algorithms that are used for enhancement comparison with the proposed method, is presented in this paper. Figures 4b and 5b presents the results obtained using histogram equalization, which is a common enhancement technique to improve the intensity contrast in images. Histogram equalization effectively spread out the most frequent intensity values of the image to improve the image contrast [13]. However, one can notice from Figs. 4b and 5b histogram equalization has inadequate effect on highly density tissues, as well as insufficient for local contrast. Hence, it is more difficult to differentiate the mass from the background and outline the shapes and edges of the mass.

Figures 6b and 7b shows the results for denoising and enhancement of mammographic images using a method proposed by Pelin Gorgel et al. [13]. In his approach denoising is based on wavelet shrinkage operator, where detail coefficients are modified and the enhancement is based on homomorphic filtering applied to approximation coefficients after taking wavelet transform of mammograms. Finally, the adaptive threshold was used to enhance the fine details of the mammographic images. However, it is clearly seen from Fig. 6b that, this method has limited effect on highly dense breast, as dense tissue and mass having almost same contrast. Therefore, it seems difficult to discriminate the mass from the background and delineate the shapes of mass, due to the same appearance of mass and dense tissue.

Figures 8a and 9a are dense-glandular mammograms, Figs. 10a, 12a and 13a are the fatty mammograms, and Fig. 11a is fatty-glandular mammogram from DDSM and MIAS database. The value of $K_c = 12$ and $t = 0.9$ is used through out the algorithm proposed in this paper is user defined obtained after several iteration. Figures 8e, 9e, 10e, 11e, 12e, and 13e shows the results of the proposed method for denoising and enhancement using shrinkage function and piecewise linear operator for different types of mammograms.

Fig. 7 a Original image, case mdb105(MAIS) **b** results obtained using method proposed by Pelin Gorgel et al. [13]
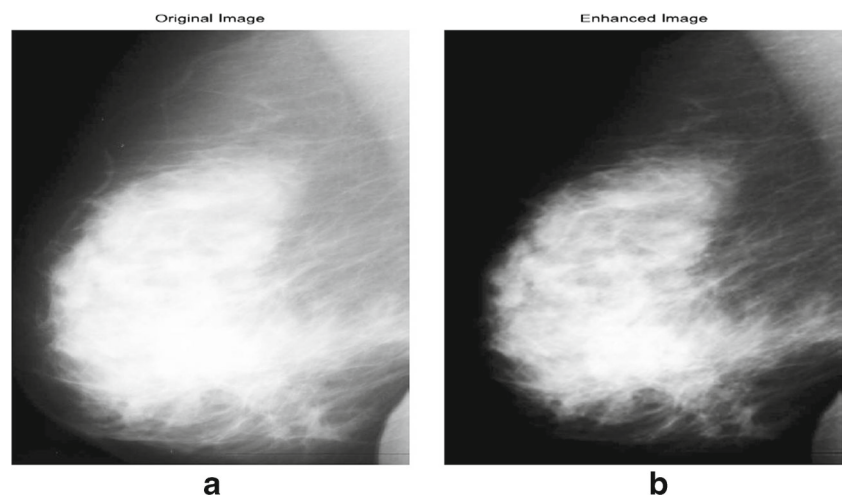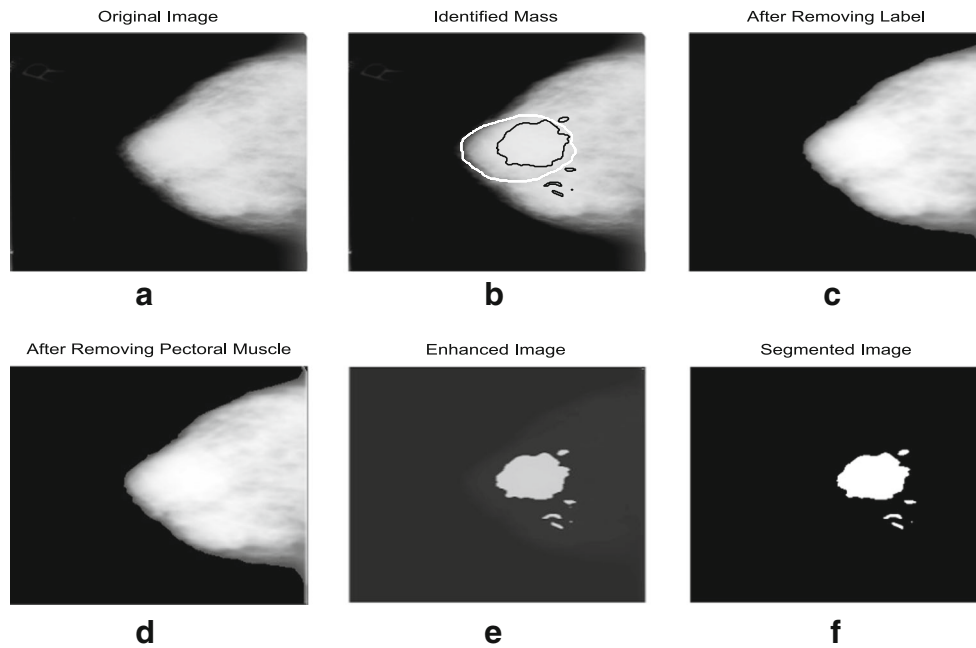
Fig. 8 **a** Original image, case B 3002 (DDSM). **b** Detected suspicious mass using proposed algorithm (*black outline*) and by radiologist (*opwhite outline*). **c** removing of artifacts. **d** removing pectoral muscle. **e** denoising and enhancement, $K_n = 12$ gain and $t = 0.9$ **f** segmented Image

It can be seen that, abnormal masses are clearly depicted for all types of mammograms (i.e., fatty, dense-glandular and fatty-glandular). The results of mass segmentation, without emphasizing the background outline the proper edges of the suspicious masses using presented adaptive threshold technique as observed in Figs. 8f, 9f, 10f, 11f, 12f and 13f. The same database has been used for the comparison of the proposed method with two different methods presented in literature, i.e. histogram equalization, and method proposed by Pelin Gorgel et al. [13], for mass enhancement as presented in Figs. 4b, 5b, 6b, and 7b. Thus, from these results, one can conclude that, results obtained using proposed method shows better distinguished masses than that of other methods. The other methods gives clear
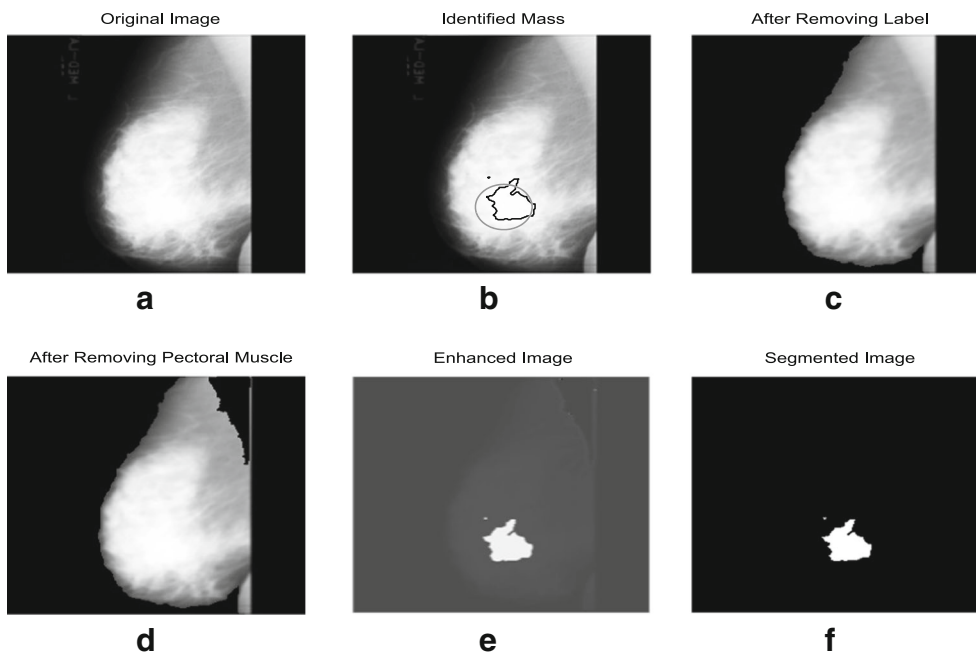

Fig. 9 **a** Original image, case mdb105 (MIAS). **b** detected suspicious mass using proposed algorithm (*black outline*) and by radiologist (*white outline*). **c** removing of artifacts. **d** removing pectoral muscle. **e** denoising and enhancement, $K_n = 12$ gain and $t = 0.9$ **f** segmented Image

Fig. 10 **a** Original image, case mdb025 (MIAS). **b** detected suspicious mass using proposed algorithm (*black outline*) and by radiologist (*white outline*). **c** removing of artifacts. **d** removing pectoral muscle. **e** denoising and enhancement, $K_n = 12$ gain and $t = 0.9$ **f** segmented Image
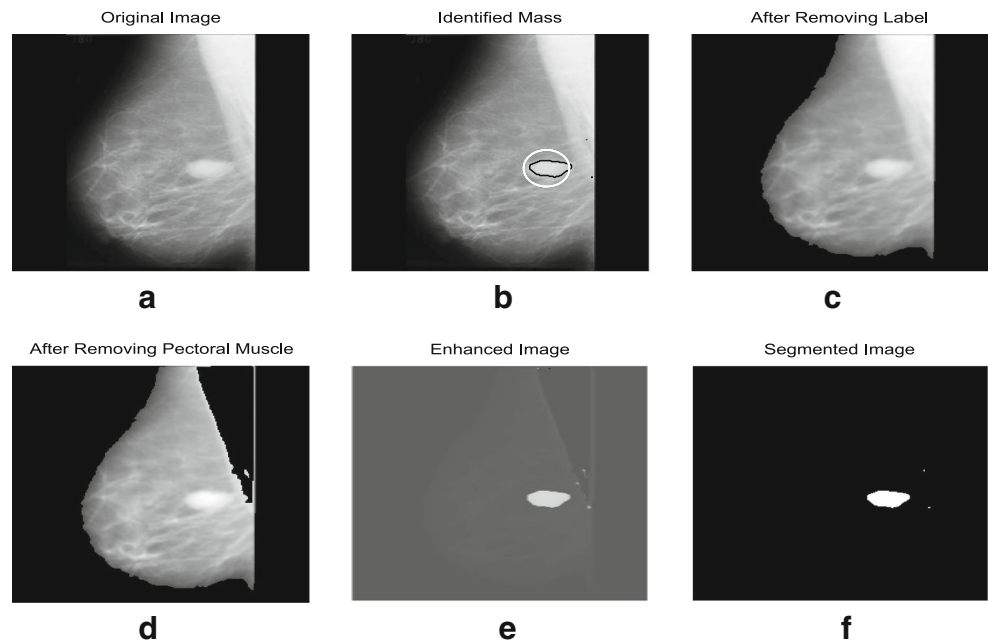
idea to have an inadequate effect on dense-glandular and fatty-glandular mammograms. Hence, it may be difficult to outline the boundaries in the case of histogram equalization and Pelin Gorgel et al. methods. Therefore, these methods may not be suitable for mass detection of highly dense mammograms. Figures 8b, 9b, 10b, 11b, 12b and 13b presents the effectiveness of the proposed method, where the black outline presents the mass detected using proposed method and the white outline shows the mass marked by a radiologist. Removal of artifacts and pectoral muscle segmentation if present can be observed in Figs. 8c, d, 9c, d,

10c, d, 11c, d, 12c, d and 13c, d. Thus, the mass enhancement process due to artifacts and the high intensity pectoral region is not affected. The method is demonstrated for CC and MLO view of the mammographic images. However, the method proposed by [13], works only for CC view, and may not work for MLO view, due to the high intensity triangular region of pectoral muscle, which may be detected as mass or abnormality.

Figures 14, 15 and 16 each having four cases were (a) in each case is the original mammograms and (b) of each case present results for mass identification for DDSM and

Fig. 11 **a** Original image, case C 0009 (DDSM). **b** detected suspicious mass using proposed algorithm (*black outline*) and by radiologist (*white outline*). **c** removing of artifacts. **d** removing pectoral muscle. **e** denoising and enhancement, $K_n = 12$ gain and $t = 0.9$ **f** segmented Image
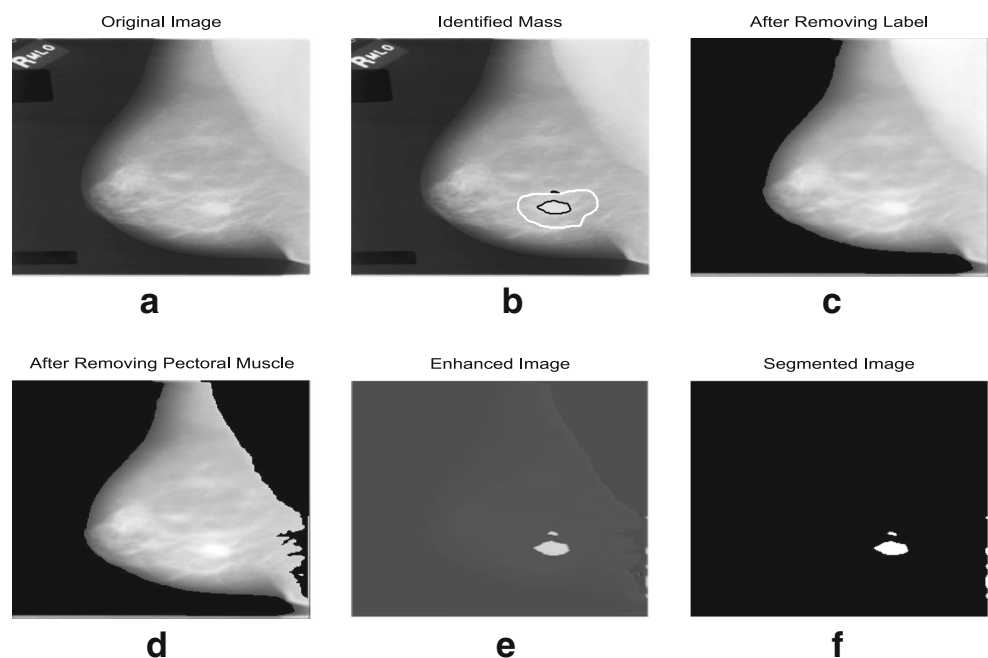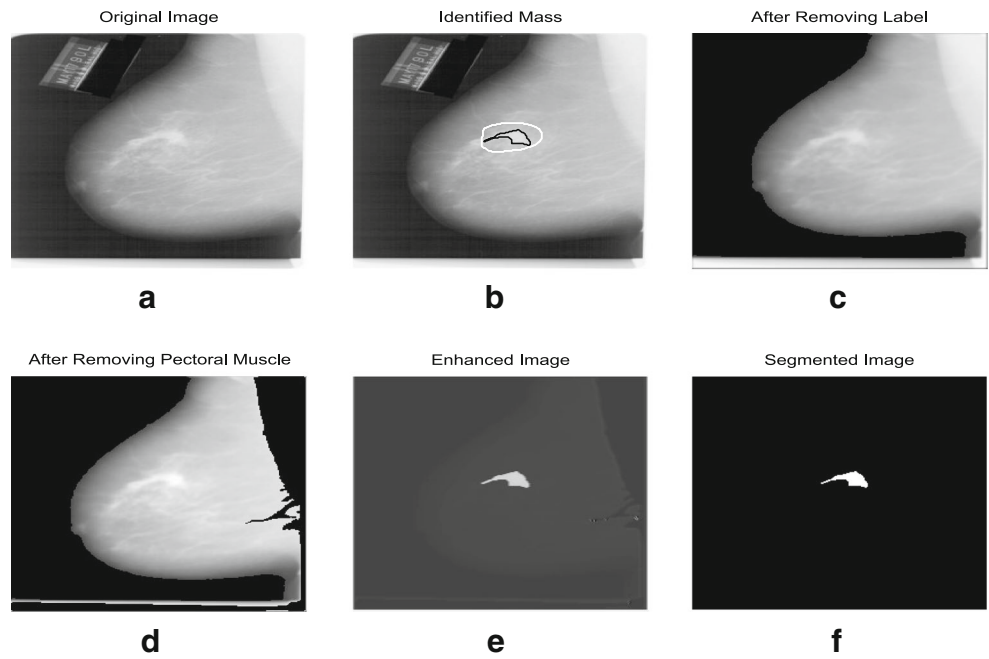
Fig. 12 **a** Original image, case A 1229 (DDSM). **b** detected suspicious mass using proposed algorithm (*black outline*) and by radiologist (*opwhite outline*). **c** removing of artifacts. **d** removing pectoral muscle. **e** denoising and enhancement, $K_n = 12$ gain and $t = 0.9$ **f** segmented Image

MIAS database using proposed method with varying shape, size, location and types of the mammographic images. The shape of mass detected by radiologist (white) and proposed method (black) have almost similar match. This emphasizes the effectiveness of the proposed method as it correctly enhance and identifies the abnormalities from the mammograms.

Discussion

To elaborate the strength of the proposed method for enhancement Fig. 17 presents two cases i.e. A 1404 and mdb104 for comparative analysis for mass enhancement. In this Fig. 17a is the original mammogram, (b) enhancement results of histogram equalization, (c) enhancement

Fig. 13 **a** Original image, case mdb271 (MIAS). **b** detected suspicious mass using proposed algorithm (*black outline*) and by radiologist (*white outline*). **d** removing pectoral muscle. **e** denoising and enhancement, $K_n = 12$ gain and $t = 0.9$ **f** segmented Image
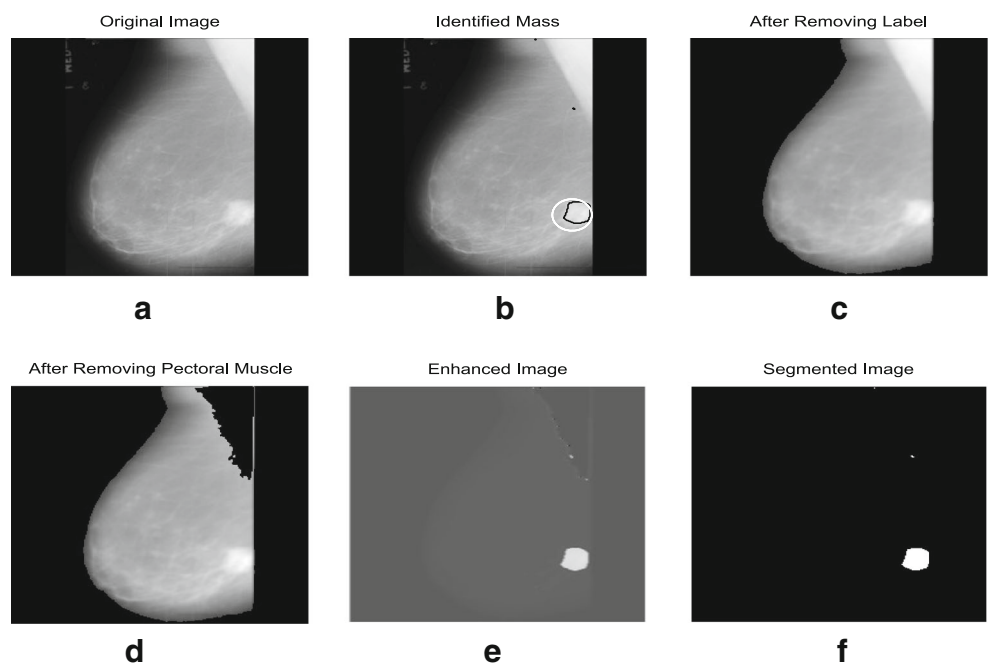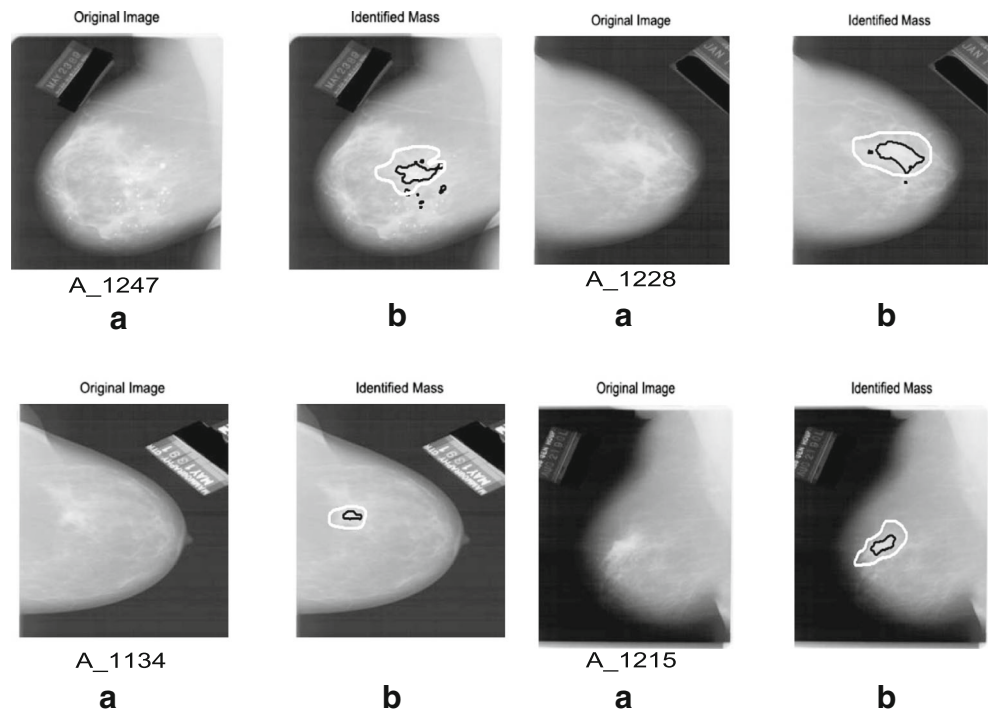
Fig. 14 **a** Original
mammograms with case
numbers. **b** comparison between
boundary detection of the mass
for DDSM database by
radiologist and by the proposed
method is given by white outline
and black outline respectively

results of Pelin Gorgel et al. method and (d) enhancement
results of proposed method. The results shows improvement
in enhancement with proposed method than other meth-
ods presented in the literature. As it can be clearly noticed
from Fig. 17b, how histogram equalization approach is
inadequate to enhance and distinguish the edges of mass.
Also one can observe that entire high contrast region is
enhanced using Pelin Gorgel et al. method, hence specific

ROI detection is difficult from mammograms, as depicted
in Fig. 17c. However from Fig. 17d mass is clearly depicted
with proposed enhancement method.

The Tables 3 and 4 illustrate the mass detection results.
Whereas, Fig. 18 presents the FROC analysis of the pro-
posed method for MIAS and DDSM database, generated by
setting different threshold. The average false positive per
image (FP/I) Verses true positive fraction (TPF) is presented

Fig. 15 **a** Original
mammograms with case
numbers. **b** comparison between
boundary detection of the mass
for MIAS database by
radiologist and by the proposed
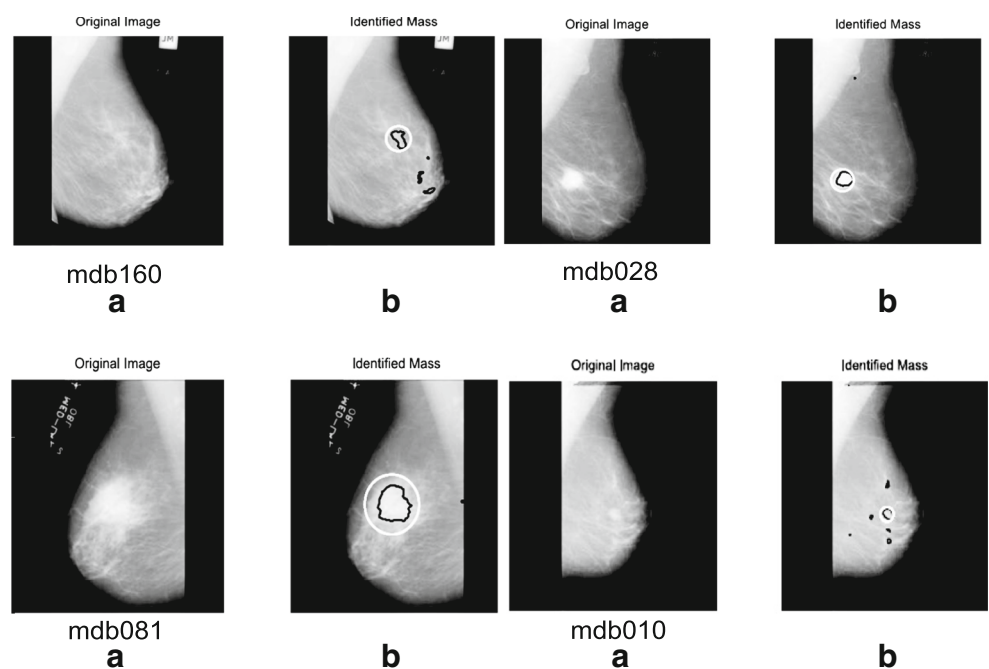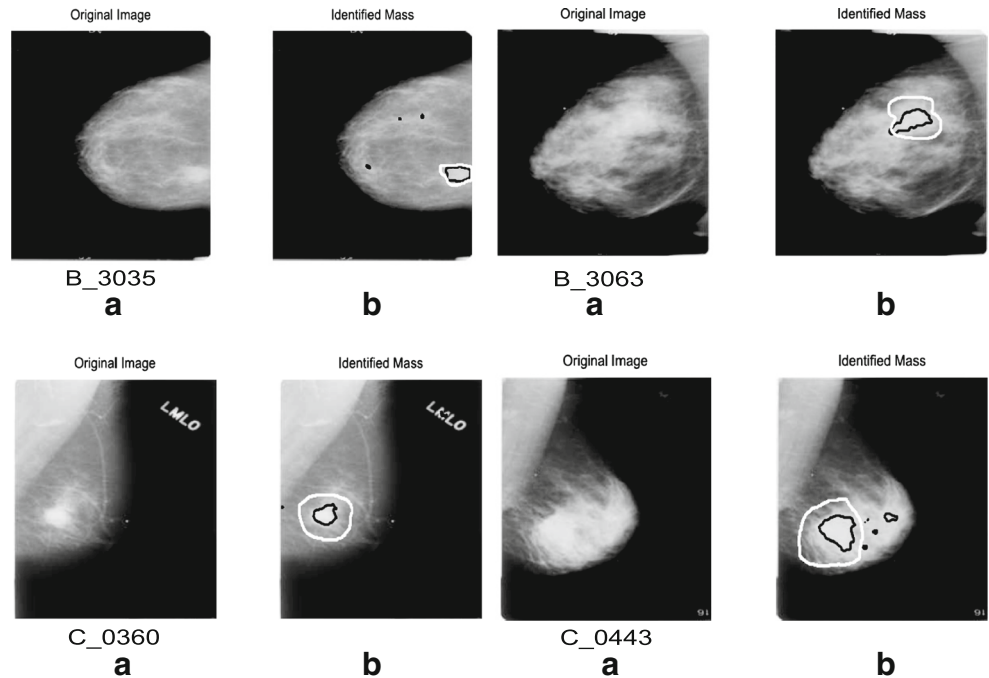algorithm is given by white
outline and black outline
respectively

Fig. 16 **a** Original mammograms with case numbers. **b** comparison between boundary detection of the mass for DDSM database by radiologist and by the proposed algorithm is given by white outline and black outline respectively

on x-axis and y-axis respectively. The TPF of 90.9 and 91 % were achieved at the rate of 2.35 and 2.1 FP/I, among 45 and 85 mammograms for MIAS and DDSM database respectively with proposed method. The method proposed by Cao et al. [4] have obtained the TPF of 90.7 % with average FP/I of 2.57 among 60 mammograms for MIAS database. The 80 % of TP performance was obtained by the method proposed by Li et al. [18] with average detection of 2 FP/I.

The detection accuracy of 80 % at 2.3 FP/I was achieved by the algorithm proposed by N. Perick et al. [27] for 168 mammograms. Yanfeng Li et al. [19] obtained the mass detection sensitivity with 85 % at the rate of 2.39 FP/I for 322 mammograms from MIAS database.

The effectiveness of the proposed method, correctly highlight the edges and enhances the suspicious region without emphasizing the structural background. Thus, the

Fig. 17 **a** Original mammograms case A 1404 (DDSM) and mdb104 (MIAS). **b** enhancement using histogram equalization. **c** enhancement using Pelin Gorgel et al. [13]. **d** enhancement using proposed algorithm
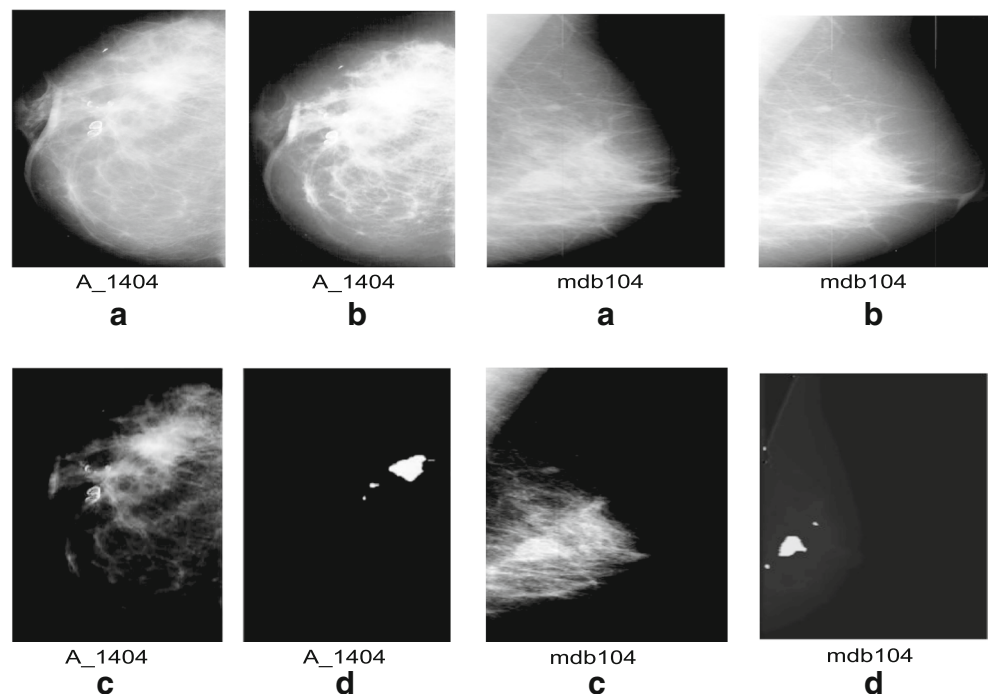
Table 3 The number of suspicious regions detected per image for proposed technique and ground truth provided by MIAS database

Case	Ground truth	Proposed method	Case	Ground truth	Proposed method	Case	Ground truth	Proposed method
mdb001	01	01	mdb081	01	02	mdb134	01	01
mdb002	01	01	mdb083	01	05	mdb145	01	04
mdb010	01	06	mdb092	01	12	mdb148	01	05
mdb013	01	00	mdb097	01	02	mdb160	01	07
mdb015	01	09	mdb102	01	03	mdb165	01	01
mdb019	01	05	mdb104	01	04	mdb178	01	02
mdb021	01	03	mdb105	01	02	mdb181	01	02
mdb023	01	06	mdb107	01	03	mdb186	01	01
mdb025	01	01	mdb115	01	02	mdb198	01	02
mdb028	01	02	mdb117	01	03	mdb213	01	02
mdb032	01	08	mdb120	01	01	mdb244	01	01
mdb058	01	07	mdb124	01	02	mdb271	01	02
mdb069	01	04	mdb127	01	03	mdb315	01	03

Table 4 The number of suspicious regions detected per image for proposed technique and ground truth provided by DDSM database

Case	Ground truth	Proposed method	Case	Ground truth	Proposed method	Case	Ground truth	Proposed method
A_1134_RCC	02	01	B_3001_LMLO	01	02	B_3077_RCC	01	01
A_1147_LCC	01	02	B_3002_RCC	01	05	B_3084_RCC	01	02
A_1215_LMLO	01	01	B_3002_RMLO	01	08	B_3084_RMLO	01	01
A_1228_RCC	01	03	B_3022_RCC	01	02	B_3106_RCC	01	03
A_1229_LMLO	02	01	B_3030_LCC	01	05	B_3108_LCC	01	01
A_1233_LCC	02	02	B_3034_LMLO	03	06	B_3109_RCC	01	02
A_1247_LCC	01	03	B_3035_LCC	01	04	B_3387_RCC	01	01
A_1247_LMLO	01	07	B_3040_RCC	02	05	B_3387_RMLO	01	01
A_1302_LCC	01	01	B_3041_LCC	01	15	B_3401_LCC	01	01
A_1412_RCC	01	02	B_3041_LMLO	01	12	B_3503_LCC	01	02
A_1468_RMLO	01	03	B_3043_LCC	02	05	B_3504_RCC	02	02
A_1481_LCC	01	02	B_3049_LCC	01	02	B_3508_RMLO	01	01
A_1483_LCC	01	03	B_3051_RCC	01	03	C_0004_RMLO	01	01
A_1491_RCC	01	04	B_3051_RMLO	01	05	C_0005_RCC	01	02
A_1498_LCC	01	00	B_3052_LCC	03	05	C_0009_RMLO	01	02
A_1511_RCC	01	05	B_3056_LCC	01	02	C_0020_LMLO	01	05
A_1515_RMLO	01	01	B_3058_LCC	01	01	C_0055_LMLO	01	02
A_1519_LCC	01	04	B_3060_RCC	02	03	C_0060_RCC	01	10
A_1537_LMLO	01	02	B_3061_RMLO	01	01	C_0066_RMLO	01	04
A_1538_LCC	01	05	B_3063_RMLO	01	01	C_0128_RCC	01	02
A_1895_RMLO	01	06	B_3075_RCC	03	04	C_0144_LCC	01	03
A_1933_LCC	01	03	B_3075_RMLO	03	03	C_0144_LMLO	01	02
C_0152_RCC	01	05	C_0154_RMLO	01	07	C_0176_LCC	01	02
C_0186_LCC	01	02	C_0339_RMLO	01	03	C_0342_LCC	01	04
C_0345_LCC	01	02	C_0360_RMLO	01	03	C_0443_LCC	01	04

LCC = *Left Cranio-Caudal view*, LMLO= *Left Medio-Lateral Oblique view*, RCC = *Right Cranio-Caudal view*, RMLO= *Right Medio-Lateral Oblique view*

Fig. 18 FROC analysis for proposed mass detection system for MIAS (*black*) and DDSM (*blue*) database
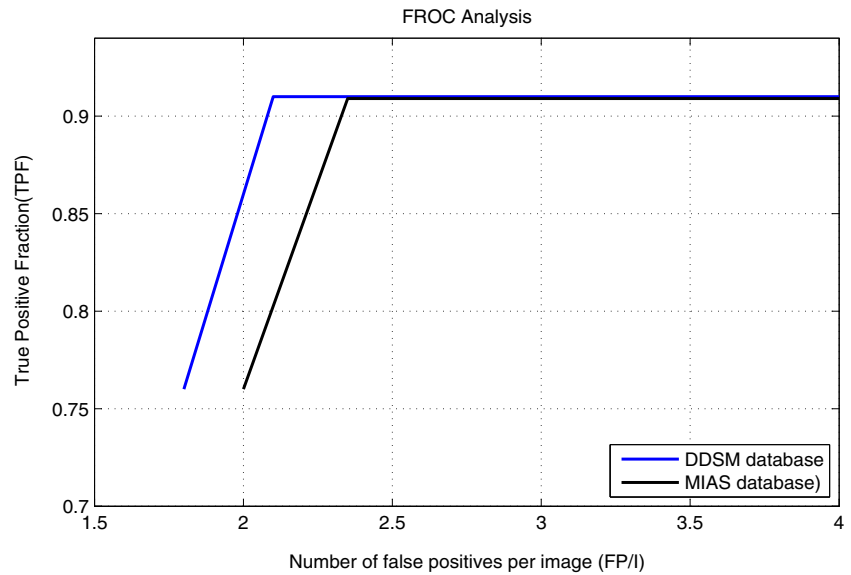
method can be known as good since it can detect the mass of varying shape, size, location and types, with 90.9 and 91 % of TPF at 2.35 and 2.1 FP/I, that includes the presence of artifacts, and pectoral muscle providing accurate enhancement and identification of mass. The suitability can be proved of the method to enhance the mass from both high and low contrast, from the results presented in the paper. Also, outline detected by algorithm (black) almost matches with radiologist (white). In some cases, false positive area can be enhanced and detected, if bright spots are available on the mammogram. This can be seen in some of the examples, where black outline is present outside the white outline, for, e.g Fig. 14b case A 1247, Fig. 15b case mdb160 and case mdb010. The contrast between breast region and pectoral muscle is indistinct, then segmentation of the pectoral muscle is difficult. This is the limitation of the proposed method.

Conclusion

This paper deals with the problem of enhancement of the mammographic images. The proposed method consists of shrinkage function and piecewise linear operator based on wavelet processing. The method includes three steps: preprocessing, wavelet based denoising and enhancement and segmentation using adaptive threshold technique for mass detection. The experimental results for enhancement and detection has proved that the shapes of the suspicious region are well preserved and clearly distinguished from high contrast regions and backgrounds without blurring the edges, which shows the effectiveness with TPF of 90.9 and 91 % at 2.35 and 2.1 FP/I for MIAS and DDSM database of proposed method. The improved results given by the proposed

method can be used as an important assist for radiologists in interpretation and early detection of breast cancer to reduce the mortality rate.

Future research work will concerns with classification of the detected mass among normal or abnormal and computation of the area of the detected mass to define the current stage of the cancer on bases of mass size detected, which may help the radiologist while taking decision and treatment.

References

1. http://www.wiau.man.ac.uk/services/MIAS/MIASweb.html.
2. http://marathon.csee.usf.edu/Mammography/Database.html..
3. American cancer society, cancer facts and figures. American Cancer Society, Atlanta, Ga, 2005-2015.
4. Cao, A., Song, Q., and Yang, X., Robust information clustering incorporating spatial information for breast mass detection in digitized mammograms. *Comput. Vis. Image Underst.* 109(1):86–96, 2008.
5. Chen, C., Liu, G., Wang, J., and Sudlow, G., Shape-based automatic detection of pectoral muscle boundary in mammograms. *J. Medical Biol. Eng.* 35(3):315–322, 2015.
6. Coifman, R.R., and Donoho, D.L. *Translation-invariant denoising*: Springer, 1995.
7. Donoho, D.L., Nonlinear wavelet methods for recovery of signals, densities, and spectra from indirect and noisy data. In: Proceedings of symposia in Applied Mathematics, volume 47, pages 173–205. Providence: American Mathematical Society, 1993.

8. Donoho, D.L., De-noising by soft-thresholding. *IEEE Trans. Inf. Theory* 41(3):613–627, 1995.

9. Fan, J., and Laine, A.F.: Contrast enhancement by multiscale and nonlinear operators, 1996.

10. Ferrari, R.J., Rangayyan, R.M., Leo Desautels, J.E., Borges, R.A., and Frere, A.F., Automatic identification of the pectoral muscle in mammograms. *IEEE Trans. Med. Imaging* 23(2):232–245, 2004.

11. Ganesan, K., Acharya, U., Chua, C.K., Min, L.C., Abraham, K., and Ng, K., Computer-aided breast cancer detection using mammograms: A review. *IEEE Rev. Biomed. Eng.* 6:77–98, 2013.

12. Gao, X., Wang, Y., Li, X., and Tao, D., On combining morphological component analysis and concentric morphology model for mammographic mass detection. *IEEE Trans. Inf. Technol. Biomed.* 14(2):266–273, 2010.

13. Gorgel, P., Sertbas, A., and Ucan, O.N., A wavelet-based mammographic image denoising and enhancement with homomorphic filtering. *J. Med. Syst.* 34(6):993–1002, 2010.

14. Hsu, W.-Y., Improved watershed transform for tumor segmentation: application to mammogram image compression. *Expert syst. Appl.* 39(4):3950–3955, 2012.

15. Kai, H., Gao, X., and Li, F., Detection of suspicious lesions by adaptive thresholding based on multiresolution analysis in mammograms. *IEEE Trans. Instrum. Meas.* 60(2):462–472, 2011.

16. Yoshitaka, K., Mathematical morphology-based approach to the enhancement of morphological features in medical images. *J. Clinical Bioinformatics* 1(1):1–10, 2011.

17. Kom, G., Tiedeu, A., and Kom, M., Automated detection of masses in mammograms by local adaptive thresholding. *Comput. Biol. Med.* 37(1):37–48, 2007.

18. Li, L., Qian, W., Clarke, L.P., Clark, R.A., and Thomas, J.A., Improving mass detection by adaptive and multiscale processing in digitized mammograms. In: Medical Imaging '99. International Society for Optics and Photonics, pp 490–498, 1999.

19. Li, Y., Chen, H., Yang, Y., Cheng, L., and Cao, L., A bilateral analysis scheme for false positive reduction in mammogram mass detection. *Comput. Biol. Med.* 57:84–95, 2015.

20. Majeed, T.F., Al-Jawad, N., and Sellahewa, H. *Breast border extraction and pectoral muscle removal in mlo mammogram images*, 2013.

21. Malek, A.A., Rahman, W.E.Z.W.A., Ibrahim, A., Mahmud, R., Yasiran, S.S., and Jumaat, A.K., Region and boundary segmentation of microcalcifications using seed-based region growing and mathematical morphology. *Procedia-Social Behavioral Scie.* 8:634–639, 2010.

22. Mallat, S., and Zhong, S., Characterization of signals from multiscale edges. *IEEE Trans. Pattern Anal. Mach. Intell.* 14(7):710–732, 1992.

23. Mallet, S.G., A theory for multiresolution signal decomposition: The wavelet representation. *IEEE Trans. Pattern Anal. Mach. Intell.* 11(7):674–693, 1989.

24. Mazurowski, M.A., Lo, J.Y., Harrawood, B.P., and Tourassi, G.D., Mutual information-based template matching scheme for detection of breast masses: From mammography to digital breast tomosynthesis. *J. Biomed. Inform.* 44(5):815–823, 2011.

25. Mencattini, A., Salmeri, M., Lojacono, R., Frigerio, M., and Caselli, F., Mammographic images enhancement and denoising for breast cancer detection using dyadic wavelet processing. *IEEE Trans. Instrum. Meas.* 57(7):1422–1430, 2008.

26. Nagi, J., Abdul K.S., Nagi, F., and Ahmed, S.K., Automated breast profile segmentation for roi detection using digital mammograms. In: Biomedical Engineering and Sciences (IECBES), 2010 IEEE EMBS Conference on, pages 87–92. IEEE, 2010.

27. Petrick, N., Chan, H.-P., Wei, D., Sahiner, B., Helvie, M.A., and Adler, D.D., Automated detection of breast masses on mammograms using adaptive contrast enhancement and texture classification. *Med. Phys.* 23(10):1685–1696, 1996.

28. Schalkoff, R.J. *Digital image processing and computer vision*. Vol. 286. New York: Wiley, 1989.

29. Shensa, M., The discrete wavelet transform: wedding the a trous and mallat algorithms. *IEEE Trans. Signal Process.* 40(10):2464–2482, 1992.

30. Soille, P. *Morphological image analysis: principles and applications*: Springer Science & Business Media, 2013.

31. Starck, J.-L., Fadili, J., and Murtagh, F., The undecimated wavelet decomposition and its reconstruction. *IEEE Trans. Image Process.* 16(2):297–309, 2007.

32. Suckling, J., Parker, J., Dance, D., Astley, S., Hutt, I., Boggis, C., Ricketts, I., Stamatakis, E., Cerneaz, N.S., Kok, S., and et al., The mammographic image analysis society digital mammogram database. In: Exerpta Medica. International Congress Series, volume 1069, pages 375–378, 1994.

33. Tai, S.-C., Chen, Z.-S., and Tsai, W.-T., An automatic mass detection system in mammograms based on complex texture features. *IEEE J. Bio. Health Inform.* 18(2):618–627, 2014.

34. Tang, J.l., Rangayyan, R.M., Xu, J., Naqa, I.E., and Yang, Y., Computer-aided detection and diagnosis of breast cancer with mammography: recent advances. *IEEE Trans. Inf. Technol. Biomed.* 13(2):236–251, 2009.

35. Yoon, J.H., and Yong Man, R.O., Enhancement of the contrast in mammographic images using the homomorphic filter method. *IEICE Trans. Inform. Syst.* 85(1):298–303, 2002.